第 33 卷第 10 期
2017 年 10 月

无 机 化 学 学 报
CHINESE JOURNAL OF INORGANIC CHEMISTRY

Vol.33 No.10
1881-1888

Al 含量对 AB_5 型储氢合金电极低温和高倍率性能的影响

汤争耀[1] 周万海[1] 朱 丁[2] 吴朝玲[1] 黄利武[1] 刘 昆[1] 陈云贵*,[1]

([1]四川大学材料科学与工程学院,成都 610065)

([2]四川大学新能源与低碳技术研究院,成都 610065)

摘要:系统地研究了 Al 含量对富 Ce 储氢合金 $MmNi_{4-x}Co_{0.7}Mn_{0.3}Al_x$($x$=0,0.1,0.2,0.3)电极综合电化学性能,尤其是对低温和高倍率性能的影响。在常温下,储氢合金电极放电容量和循环性能均随着 Al 含量的增加而增加,而高倍率放电性能严重下降。−20 ℃时,放电容量仍随着 Al 含量的增加而增加,但在−40 ℃下放电容量随之严重衰退。电化学动力学结果表明,常温下高 Al 合金高倍率性能的降低主要是由于电极表面电荷转移过程的恶化;低温−40 ℃下,Al 同时降低了合金电极的表面电催化活性以及体相 H 扩散能力,严重恶化电极过程动力学,从而导致了高 Al 合金极低的容量及电压输出。考虑到各电极的综合电化学性能,$MmNi_{3.8}Co_{0.7}Mn_{0.3}Al_{0.2}$ 为最佳的成分配比。

关键词:AB_5 型储氢合金;低温电化学性能;Al 替代;镍氢电池;电化学动力学

中图分类号:TB331 **文献标识码**:A **文章编号**:1001-4861(2017)10-1881-08

DOI:10.11862/CJIC.2017.228

Effects of Al Content on Low-Temperature and High-Rate Performance of $MmNi_{4.0-x}Co_{0.7}Mn_{0.3}Al_x$ Alloys

TANG Zheng-Yao[1] ZHOU Wan-Hai[1] ZHU Ding[2] WU Chao-Ling[1]

HUANG Li-Wu[1] LIU Kun[1] CHEN Yun-Gui*,[1]

([1]*College of Materials Science and Engineering, Sichuan University, Chengdu* 610065, *China*)

([2]*Institute of New Energy and Low-Carbon Technology, Sichuan University, Chengdu* 610065, *China*)

Abstract: Effects of Al content on the comprehensive electrochemical performance of Ce-rich $MmNi_{4-x}Co_{0.7}Mn_{0.3}Al_x$ (x=0, 0.1, 0.2, 0.3) hydrogen storage alloys, particularly the low-temperature and high-rate capacity have been systematically investigated. At room temperature, both the discharge capacity and cycling stability of the electrode increase with the Al content increases, but the high-rate dischargeability seriously deteriorates. The discharge capacity still increases with the increase of Al content at −20 ℃, but gradually deteriorates when the temperature drops down to −40 ℃. Electrochemical kinetics results demonstrate that the high-rate capacity recession of the high-Al alloy at room temperature is contributed to the deterioration of the charge-transfer process. When the temperature drops down to −40 ℃, Al deteriorates both the surface catalytic ability and the bulk hydrogen diffusion ability, leading to the severe drop of discharge capacity and potential of the high-Al alloy. Based on the comprehensive electrochemical properties of the electrodes, the optimal composition of $MmNi_{4-x}Co_{0.7}Mn_{0.3}Al_x$ is obtained when x=0.2.

Keywords: AB_5-type hydrogen storage alloy; low-temperature electrochemical performance; aluminum substitution; nickel metal hydride battery; electrochemical kinetics

收稿日期:2017-05-26。收修改稿日期:2017-09-04。

四川省科技创新苗子工程(No.2017RZ0033)资助项目。

*通信联系人。E-mail:ygchen60@aliyun.com

0 Introduction

Nowadays, in order to cope with global warming and air pollution, as well as the growing needs of mobile or stationary power supplies for portable electronics, electric vehicles and power grids, the development of rechargeable batteries has caught wide attentions to researchers. Nickel/metal hydride (Ni/MH) batteries have evolved quickly as popular energy storage systems, particularly in the high-power market, such as portable power tools, hybrid electric vehicles (HEV). As of January 2017, global hybrid sales are led by the Prius family, with cumulative sales of 6.036 1 million units (excluding plug-in hybrids) representing 60% of the 10 million hybrids sold worldwide by Toyota and Lexus[1]. Ni/MH battery dominates HEV applications through a combination of desirable performance attributes such as high energy and power, an excellent range of operating temperatures, and low cost. In the last three decades, Ni/MH batteries have achieved great progress in the limits of the low self-discharge[2-3], long life cycle[4-5], low cost[6-7], high energy[8-9], and wide temperature performance[10-11]. For practical applications, especially in HEV, modern military electronic devices, space applications and gelid areas, it is necessary for Ni/MH batteries to work satisfactorily at the temperature down to −40 ℃[12-13]. MH electrode alloy, as the key material in Ni/MH battery generally becomes to the main limits of the batterys charge/discharge behavior at lower temperatures, because of the severe deterioration in electrochemical kinetics.

Generally, the electrochemical kinetics of the MH electrode mainly contains two aspects: the charge-transfer process on the alloy surface and the hydrogen diffusion process in the bulk of the alloy[14-16]. The charge-transfer process is generally related to the surface state of the electrode. By now, various feasible economical approaches, such as electrolyte adjustment[16-17], nano-nickel powder additives[18] and duplex surface hot-alkali treatments[19], have been employed to accelerate charge transfer process. Meanwhile, multi-alloying of the alloys[11, 20-24] is normally regarded as an efficient approach to adjust both the inherent thermodynamic stability and electrochemical kinetics. Al is regarded as an essential element of the hydrogen storage alloy for commercial Ni/MH battery, due to its good thermodynamic property, excellent corrosion resistance at room temperature[25]. And the amount of Al substitution is generally controlled in the range of 0.1~0.3. However, the electrochemical kinetics of the alloy electrode will be impeded by the formation of the Al oxide film on the metal hydride surface[26]. This may make the low-temperature and high-rate dischargeability of MH electrode severely deteriorate. Therefore, the adjustment of the Al content is critical to the optimization of the low-temperature and high-rate performance of the MH electrode.

Based on above, the Ce-rich mischmetal was employed to ensure the thermodynamic stability of the low-temperature hydrogen storage alloy. $MmNi_{4-x}Co_{0.7}Mn_{0.3}Al_x$ (x=0, 0.1, 0.2, 0.3; Mm: Ce-rich mischmetal, consisting of Ce, La and Pr) alloys were designed to optimize low-temperature and high-rate performance of the electrode. The effects of Al content on the comprehensive electrochemical performance, particularly the low-temperature and high-rate capacity were systematically studied.

1 Experimental

The active material $MmNi_{4-x}Co_{0.7}Mn_{0.3}Al_x$($x$=0, 0.1, 0.2, 0.3) alloys were prepared by arc melting technology. The purity of all the starting elemental metals in this experiment was over 99.5%(w/w). The samples were arc-melted into button-shaped ingots under argon atmosphere and re-melted for four times to ensure compositional homogeneity. Part of the as-cast ingot were mechanically crushed and ground into powders. Alloy powders with a dimension of 200-mesh (<75 mm) were used for electrochemical tests, and those with a size of 400-mesh (<38 mm) were used for X-ray diffractometer (XRD) analysis. Crystallographic characteristics of the alloys were examined by XRD (DX-2600 equipment with Cu $K\alpha$ radiation at a sweep rate of 0.04°·s^{-1}, λ=0.015 418 nm, U=35 kV, I=25

mA, 2θ=20°~80°).

Each metal hydride electrode was prepared by cold-pressing the mixture of 0.12 g of alloy powder with 0.36 g of nickel powder (T255, CAN. INCO) into a pellet (d=10 mm, h=1 mm) under a pressure of 65 MPa. Electrochemical measurements were performed in a half-cell consisting of the metal hydride working electrode, a sintered $Ni(OH)_2$/NiOOH counter electrode and a Hg/HgO reference electrode immersed in 6 mol·L^{-1} KOH electrolyte. Each electrode was fully activated at room temperature with a 0.2C (60 mA·g^{-1}) charge/discharge current density. The discharge cut-off potential of the electrode was −0.6 V (vs Hg/HgO), except when the temperature reached −40 ℃, or the discharge rate was above 5C (1 500 mA·g^{-1}), it was −0.55 V (vs Hg/HgO). For the low-temperature electrochemical measurements, electrodes were charged under 0.2C at room temperature and sustain for 7 h and then discharged at −20 and −40 ℃ with 0.2C, respectively, after keeping the testing system at a constant temperature for 4 h by using a low-temperature equipment (DWB 202).

Electrochemical impedance spectra (EIS) were measured using a sine perturbation signal of 5 mV in the frequency range of 10 kHz ~5 mHz. Exchange current density (I_0) was measured by linear polarization (LP) curves, scanning electrode potential at the rate of 0.1 mV·s^{-1} from −5 to 5 mV. Prior to all of the electrochemical kinetics analysis (performed by Parstat-2273 electrochemical potentiostat), the electrodes were discharged to 50% depth of discharge (50% DOD) and then rest for 2 h. Hydrogen diffusion coefficient (D) was estimated by the constant potential step (CPS) method, and the test electrodes were discharged at a constant potential of E=−0.6 V (vs Hg/HgO) for 3 600 s after 100% charge state.

2 Results and discussion

2.1 Microstructure

Details of the effects of Al on the crystal structure characteristics of the AB_5-type hydrogen storage have been previously reported[25-28]. Here, a revisiting of XRD test is necessary to ensure the basic phase composition, and the actual measured XRD patterns and lattice parameters of the alloys are shown in Fig.1 and Table 1, respectively. As shown in Fig.1, the diffraction peaks of all the alloys are completely appointed to those of $LaNi_5$ phase with a hexagonal $CaCu_5$ crystal structure. The lattice constant a and c increase with the increase of Al content, and correspondingly leads to the increase of unit-cell volume. The reason is that the metallic radius of Al (0.143 nm) is litter larger than that of Ni (0.124 nm). In addition, the anisotropy (ratios of c/a) increases via Al substituting, which means higher cycle stability for the high-Al alloy according to our previous work[26]. All of the results have a good consistency with reports elsewhere[25-29].

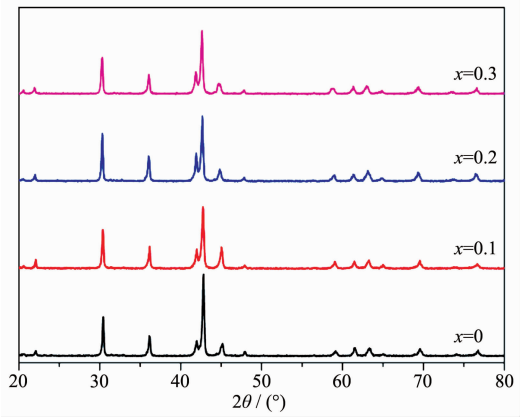

Fig.1 XRD patterns of the $MmNi_{4-x}Co_{0.7}Mn_{0.3}Al_x$($x$=0, 0.1, 0.2, 0.3) hydrogen storage alloys

Table 1 Lattice parameters of $MmNi_{4-x}Co_{0.7}Mn_{0.3}Al_x$($x$=0, 0.1, 0.2, 0.3)

Sample	Lattice constant			Cell volume / nm^3
	a / nm	b / nm	c / nm	
x=0	0.496 4(0)	0.401 2(5)	0.080 8(2)	0.085 63
x=0.1	0.496 7(2)	0.402 0(3)	0.080 9(3)	0.085 89
x=0.2	0.497 3(8)	0.403 5(2)	0.081 1(4)	0.086 45
x=0.3	0.497 4(8)	0.404 9(4)	0.081 4(9)	0.086 75

2.2 Electrochemical performance

2.2.1 Room-temperature electrochemical behavior

The room-temperature electrochemical properties of the $MmNi_{4.0-x}Co_{0.7}Mn_{0.3}Al_x$ (x=0, 0.1, 0.2, 0.3) alloys are shown in Table 2. All the alloy electrodes can be fully activated within 3 times at room temperature. The maximum discharge capacity at both 0.2 and 1C increases with the increase of Al content. This is inconsistent with the results of previous work[25-26]. Here, the Ce-rich AB_5-type alloys which possess lower thermodynamic stability are used for electrode material. The poor thermodynamic stability make the Al-free alloy hardly hydrogenate, and the charge potential prematurely reaches the hydrogen evolution reaction (HER) potential (E_{HER}), leading to a poor charge acceptance ability. Fig.2a and 2b illustrate the charge and discharge curves of the electrodes at 20 ℃ with 0.2C. The potential of the x=0 electrode polarizes to its maximum value rapidly, and it is hard to distinguish the hydride formation reaction (HFR) plateau and HER plateau. According to our previous work[25], The potential difference ($E_{HER}-E_{mid,c}$, $E_{mid,c}$ is the middle charge plateau potential) between the HFR plateau and HER plateau can be used to evaluate the charge acceptance ability. As shown in Fig.2c, the $E_{HER}-E_{mid,c}$ value increases gradually with the increase of Al content, correspondingly leads to an improved discharge capacity. In addition, the value of $E_{mid,c}-E_{mid,d}$ ($E_{mid,d}$ is the middle discharge plateau potential) can be used to evaluate the charge/discharge polarization of the electrode[30]. As shown in Fig.2c, the $E_{mid,c}-E_{mid,d}$ values increase from 0.051 1 V for x=0 alloy to 0.083 7 V for x=0.3 alloy. This is in good agreement with previous report that charge/discharge polarization increases with the increase of Al content due to the oxide film formed by Al[26].

Fig.3 shows the high-rate dischargeability (HRD) of the $MmNi_{4-x}Co_{0.7}Mn_{0.3}Al_x$($x$=0, 0.1, 0.2, 0.3) alloys at room temperature, and the HRD value can be calculated from the following equation:

$$HRD_d=\frac{C_d}{C_{60}}\times 100\%$$

Where C_{60} denotes the discharge capacity at the discharge current density of 60 mA·g^{-1}, and C_d denotes the discharge capacity at the current density of 60, 300, 600, 900, 1 500 and 3 000 mA·g^{-1}. It is interesting that the x=0 and x=0.1 alloys possess higher discharge capacity at 1C than that at 0.2C. This is related to the higher hydrogen desorption plateau pressure in Ce-rich-based alloys, leading to poor thermodynamic stability in $MmNi_{4.0-x}Co_{0.7}Mn_{0.3}Al_x$ (x=0, 0.1, 0.2, 0.3) alloys. This makes the x=0 and x=0.1

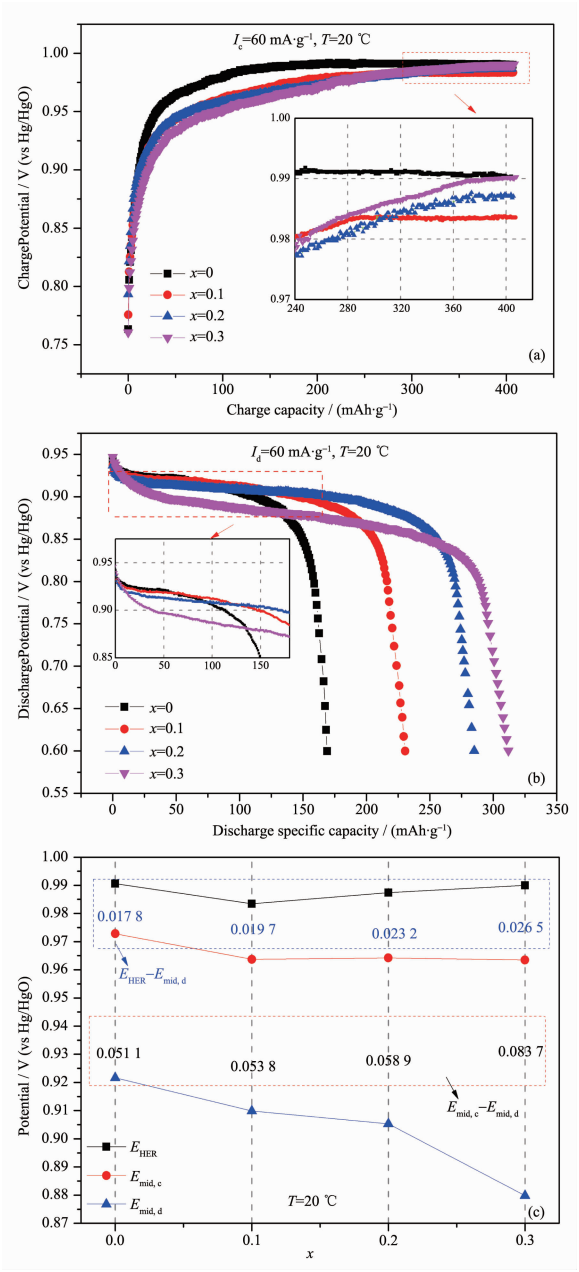

Fig.2 Charge curves (a), discharge curves (b) and middle charge/discharge plateau potential and hydrogen evolution reaction potential (c) at 20 ℃

Table 2　Electrochemical properties of $MmNi_{4-x}Co_{0.7}Mn_{0.3}Al_x$($x$=0, 0.1, 0.2, 0.3)

Sample	N_a[a]	$C_{0.2C}$[b] / (mAh·g^{-1})			Capacity / (mAh·g^{-1})				LTD_{-40} / %	HRD_{1500} / %	S_{60} / %
		20 ℃	−20 ℃	−40 ℃	1C	2C	5C	10C			
x=0	2	179.2	181.8	114.8	197.7	163.6	136.7	52.1	64.1	76.3	79.2
x=0.1	3	239.6	218.4	132.7	242.6	206.6	144.9	49.5	55.4	60.5	91.6
x=0.2	3	298.1	252.4	112.9	267.3	253.2	166.4	51.9	37.9	55.8	92.1
x=0.3	3	306.2	250.3	28.1	278.4	232.9	162.0	30.5	9.2	52.9	95.2

[a] Cycle numbers needed to reach the maximum discharge capacity of the electrode at 60 mA·g^{-1}; [b] Maximum discharge capacity at a discharge current density of 60 mA·g^{-1}.

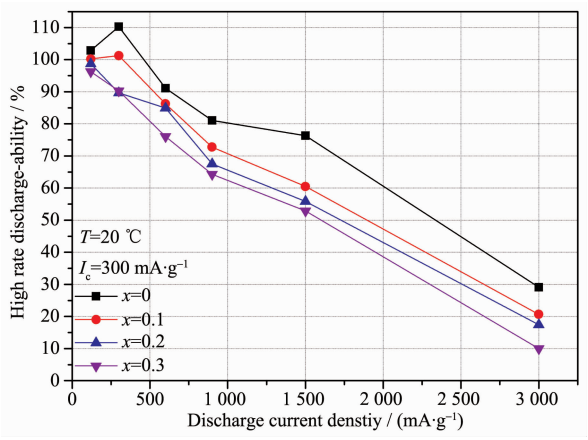

Fig.3　High-rate discharge capacity of $MmNi_{4.0-x}Co_{0.7}Mn_{0.3}Al_x$ (x=0, 0.1, 0.2, 0.3) alloy electrodes at 20 ℃

electrodes have spontaneous escape hydrogen tendency, causing a reversible loss of capacity. At 1C, the electrode discharge time is shorter, reducing the loss of self-discharge capacity. With the current density increases gradually, the discharge capacity of each alloy declines. Although the high-rate discharge capacity of high-Al alloy is higher than that of low-Al alloy, the HRD value decreases with the increase of Al content. When discharged at 5C, the discharge capacity of x=0.3 alloy is 162.0 mAh·g^{-1}, significantly higher than 136.7 mAh·g^{-1} of x=0 alloy. But the value of HRD_{1500} decreases from 76.3% (x=0) to 52.9 (x=0.3). Particularly at 10C, the high-Al (x=0.3) alloy barely discharges, and the HRD_{3000} is only 9.96%.

2.2.2　Low-temperature performance

Fig.4 shows the discharge curves of the $MmNi_{4-x}Co_{0.7}Mn_{0.3}Al_x$($x$=0, 0.1, 0.2, 0.3) alloy electrodes at −20 and −40 ℃. It can be seen from the Fig.4a that the change trend of the discharge capacity at −20 ℃ is consistent with that at the room temperature, *i.e.*, the discharge capacity of the electrode increases with the increase of Al content. However, it is different when the temperature drops down to −40 ℃. There is a severe decline of discharge capacity for the high-Al alloy. The x=0.3 alloy only can contribute a discharge capacity of 28.1 mAh·g^{-1}. Thus the discharge capacity decreases from 114.8 mAh·g^{-1} (x=0) to 28.1 mAh·g^{-1} (x=0.3). Here, the low-temperature dischargeability (LTD), which is an important reference index for low-temperature battery, is employed to evaluate the low-temperature performance. It can be expressed by the

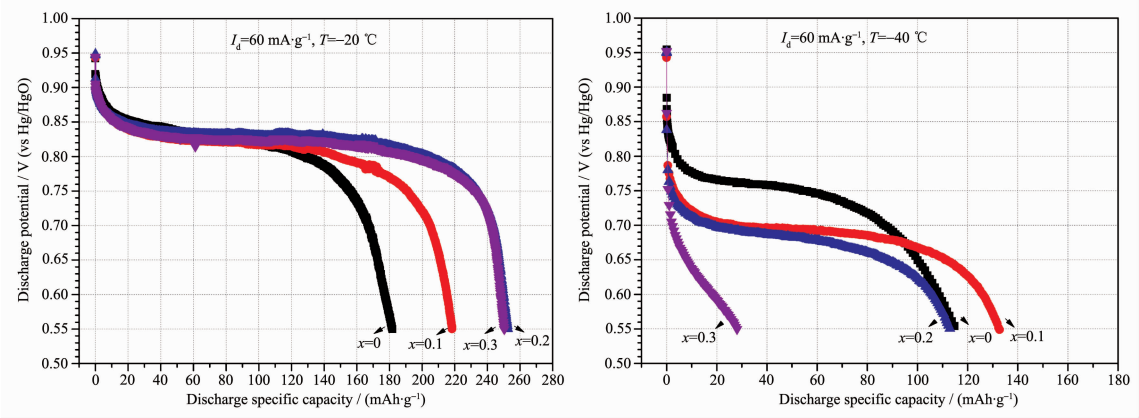

Fig.4　Discharge characteristics of $MmNi_{4-x}Co_{0.7}Mn_{0.3}Al_x$($x$=0, 0.1, 0.2, 0.3) at −20 ℃ (a) and −40 ℃ (b)

following formula:

$$LTD_{-40}=\frac{C_{-40}}{C_{20}}\times 100\%$$

Where C_{20} and C_{-40} represent the discharge capacity at the discharge current density of 60 mA·g^{-1} at 20 and −40 ℃, respectively. As shown in Table 2, the values of LTD_{-40} decrease from 64.1% for Al-free alloy to 9.2% for x=0.3 alloy. This indicates that the decrease of Al content is beneficial to improve the low-temperature performance of the alloy. In addition, as shown in Fig. 4b, there is a remarkable drop for the discharge plateau potential. The decrease of discharge potential is expected because the decreased temperature contributes to a drop in the hydrogen desorption plateau in gas-solid reactions. And the strong polarization turns to the limiting factor at lower temperatures based on the previous study[19,30]. The discharge potential decreases obviously with the increase of Al content, it decreases from 0.738 1 V for the Al-free alloy to 0.617 1 V for the x=0.3 alloy. Therefore, the low-Al design is conducive to reducing the electrode polarization, improving the low-temperature performance of the alloy.

2.3 Electrochemical kinetics

The discharge ability of the electrode severely decays at extreme low temperatures and high rate, which is attributed to the following polarization: (1) resistance polarization due to the increase in the internal resistance (the electrolyte resistance and oxide film impedance); (2) electrochemical polarization due to the increase in the faradaic impedance (the charge-transfer resistance and the hydrogen diffusion impedance); and (3) concentration polarization due to micro-area consumption of the electrolyte. Here, the alloy electrodes were measured in a liquid-rich half-cell with 6 mol·L^{-1} KOH solutions to relieve the concentration polarization, and the electrochemical polarization is intensively discussed in this work.

EIS measurement is an effective approach to study the electrode kinetics as well as the reaction mechanism of the MH electrode. A novel explanation of EIS response in metal hydride electrodes was demonstrated by Yang et al.[21] to study polarization at low temperature. It found out that the bulk resistance (R_b) of the cell increases seriously at low temperatures, which accounts for the internal resistance increase and subsequently stronger ohm polarization; and the charge-transfer process at the alloy electrolyte interface is limited seriously at extremely low temperatures. Fig.5 presents the Nyquist plots of $MmNi_{4-x}Co_{0.7}Mn_{0.3}Al_x$ (x=0, 0.1, 0.2, 0.3) alloy electrodes at 20, −20 and −40 ℃, respectively. The proposed model of the equivalent circuit using the circuit description code (CDC)[21] is shown in Fig.5a, where R_b is the bulk resistance, which is composed of the resistance of the separator, electrode, electrolyte as well as the contact resistance; C_{ol} and R_{ol} are the oxide layer capacitance and resistance, respectively; C_{dl} is the double layer capacitance; R_{ct} represents the charge transfer resistance and Z_w denotes the Warburg diffusion impedance due to the diffusion of hydrogen. ZSimpWin 3.21 software was used to fit the experimental data using this CDC, and the results are shown in Table 3 and Fig.5. The R_{ct} values increase with the decrease of temperature. Using the x=0.3 alloy as an example, the R_{ct} increases from 1.05 Ω at 20 ℃ to 21.51 Ω at −40 ℃. Yet again, the rise of R_{ct} proved that the charge transfer process on the alloy surface is greatly limited at extremely low temperature, which leads to the poor LTD. In addition, the R_{ct} values gradually increase with the increase of Al content at 20 ℃ and −40 ℃. This can be attributed to the accumulation of the oxidation layer via partial Al

Table 3 Kinetics parameters of electrodes at 20, −20 and −40 ℃

Sample	R_{ct} / Ω			I_0 / (A·g^{-1})			D / (cm^2·s^{-1})	
	20 ℃	−20 ℃	−40 ℃	20 ℃	−20 ℃	−40 ℃	20 ℃	−40 ℃
x=0	0.47	3.13	7.72	0.172	0.056	0.034	11.8×10^{-12}	6.27×10^{-12}
x=0.1	0.63	3.57	10.28	0.156	0.052	0.023	12.2×10^{-12}	5.16×10^{-12}
x=0.2	0.77	4.87	12.88	0.146	0.039	0.022	17.6×10^{-12}	3.41×10^{-12}
x=0.3	1.05	6.79	21.51	0.131	0.037	0.012	18.2×10^{-12}	1.12×10^{-12}

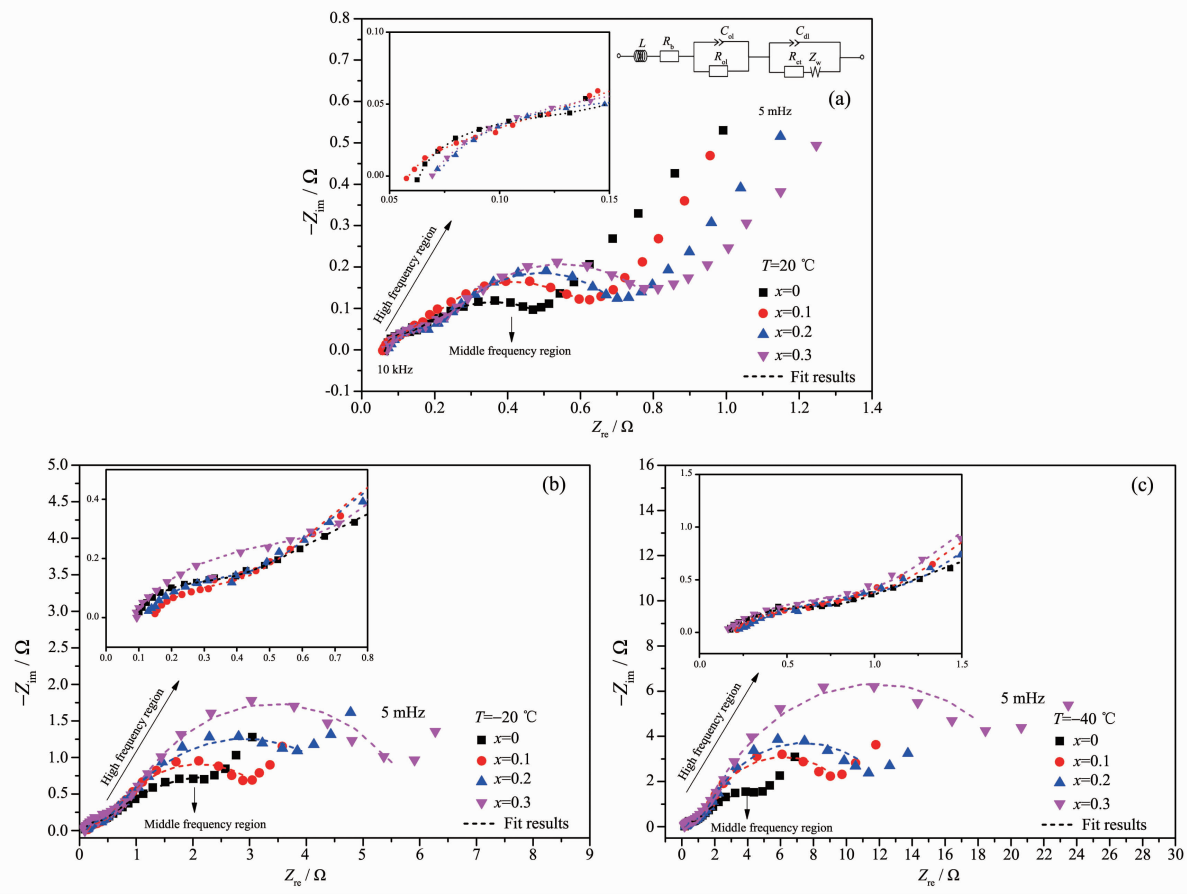

Fig.5　Nyquist plots of the alloy electrodes after activated: (a) at 20 ℃, (b) at −20 ℃, (c) at −40 ℃

substitution, and consequently causes the stronger polarization.

Conventionally, the exchange current density (I_0) which is another method that can be used to study the charge transfer process and the bulk hydrogen diffusion coefficient (D) are used to study the source of LTD and high-rate output change. Details of their computing method can be found in our previous work[19]. The I_0 and D values are presented in Table 3. Obviously, I_0 severely decreases with a decrease in the temperature and the increase of Al content, which is in accordance with the change of R_{ct}, HRD and LTD. Therefore, Al has adverse effect on the surface charge transfer process, consequently leads to the decline in HRD and LTD. In addition, the D values sharply decline at −40 ℃ with the increase of Al content. And the D value of the x=0.3 alloy is only 1.12. This may be related to the low concentration gradient of hydrogen in high-Al alloy. The charge transfer process of the high-Al alloy is limited, leading to barely discharge at −40 ℃. Consequently, the slight difference in the concentration of hydrogen between the surface and the bulk of alloy seems to offer relatively lower driving force for the diffusion of hydrogen. Therefore, we can confirm that both the hydrogen diffusion in the bulk and the charge transfer process on the alloy electrolyte interface are limited seriously at extremely low temperatures. Increasing the Al content reduces both I_0 and D at extremely low temperatures and consequently cuts down the LTD.

3　Conclusions

In summary, the following conclusions can be drawn:

With the raise of charge acceptance ability and anti-corrosion property via Al substitution, the discharge capacity and cycling stability increase at room temperature. However, Al adversely affects the

surface charge transfer process, increasing the content of Al reduces I_0, and increases R_{ct}, consequently leads to the decline in HRD. When the temperature drops down to −40 ℃, Al adversely affects both the surface catalytic ability and the bulk hydrogen diffusion ability, leading to the severe drop of discharge capacity and potential of the high-Al alloy. Based on the comprehensive electrochemical properties of the electrodes at various temperatures, an optimum alloy electrode is obtained when x=0.2.

References:

[1] https://en.wikipedia.org/wiki/Hybrid_electric_vehicle

[2] Young K, Nei J. *Materials*, **2013**,**6**:4574-4608

[3] Kong L, Chen B, Young K, et al. *J. Power Sources*, **2012**, **213**:128-139

[4] Liu Y, Pan H, Gao M, et al. *J. Mater. Chem.*, **2011**,**21**:4743-4755

[5] Young K, Wong D F, Wang L, et al. *J. Power Sources*, **2015**, **277**:426-432

[6] Sun J, Fan Y, Liu B, et al. *J. Alloys Compd.*, **2015**,**641**:148-154

[7] Wei X, Liu S, Dong H, et al. *Electrochim. Acta*, **2007**,**52**:2423-2428

[8] Young K, Ouchi T, Lin X, et al. *J. Alloys Compd.*, **2016**, **655**:50-59

[9] Li M H, Zhu Y F, Yang C, et al. *Int. J. Hydrogen Energy*, **2015**,**40**:13949-13956

[10]Yao Q, Zhou H, Wang Z, et al. *J. Alloys Compd.*, **2014**,**606**:81-85

[11]Balogun M S, Wang Z M, Zhang H G, et al. *J. Alloys Compd.*, **2013**,**579**:438-443

[12]Erbacher J K. *J. Power Sources*, **1999**,**80**:265-271

[13]Ye H, Xia B, Wu W, et al. *J. Power Sources*, **2002**,**111**:145-151

[14]Senoh H, Hara Y, Inoue H, et al. *Electrochim. Acta*, **2001**, **46**:967-971

[15]TAO Ming-Da(陶明大), CHEN Yun-Gui(陈云贵), WU Chao-Ling(吴朝玲), et al. *J. Rare Earths*(稀土学报), **2004**,**22**:882-886

[16]ZHANG Xiao-Yan(张晓燕), CHEN Yun-Gui(陈云贵), TAO Ming-Dao(陶明大), et al. *J. Rare Earths*(稀土学报), **2008**, **26**:402-405

[17]Shen X, Chen Y G, Tao M D, et al. *Electrochim. Acta*, **2009**,**54**:2581-2587

[18]Ma Z W, Zhou W H, Wu C L, et al. *J. Alloys Compd.*, **2016**,**660**:289-296

[19]Zhou W H, Tang Z Y, Zhu D, et al. *J. Alloys Compd.*, **2016**, **692**:364-374

[20]LI Rong(李蓉), WU Jian-Min(吴建民), ZHOU Shao-Xiong(周少雄), et al. *J. Rare Earths*(稀土学报), **2006**,**24**:341-345

[21]Yang H, Chen Y G, Tao M D, et al. *Electrochim. Acta*, **2010**, **55**:648-655

[22]Young K, Ouchi T, Reichman B, et al. *J. Alloys Compd.*, **2011**,**509**:3995-4001

[23]Young K, Ouchi T, Reichman B, et al. *J. Alloys Compd.*, **2011**,**509**:7611-7617

[24]Shen X, Chen Y G, Tao M D, et al. *Int. J. Hydrogen Energy*, **2009**,**34**:2661-2669

[25]Zhou W H, Ma Z W, Wu C L, et al. *Int. J. Hydrogen Energy*, **2015**,**40**:10200-10210

[26]Zhou W H, Ma Z W, Wu C L, et al. *Int. J. Hydrogen Energy*, **2016**,**41**:1801-1810

[27]Yang X G, Liaw B Y. *J. Power Sources*, **2001**,**102**:186-197

[28]Bliznakov S, Lefterova E, Dimitrov N, et al. *J. Power Sources*, **2008**,**176**:381-386

[29]Kumar E A, Maiya M P, Murthy S S, et al. *J. Alloys Compd.*, **2009**,**470**:157-162

[30]Zhou W H, Zhu D, Tang Z Y, et al. *J. Power Sources*, **2017**, **343**:11-21